

Design and simulation of a conformal optical window pair by the quasi-quantitative Schlieren measurement in a cylindrical isolator

Yang Ou^{a,b,c}, Yifan Dai^{a,b,c}, Shanyong Chen^{a,b,c}, Xiaoqiang Fan,^d
Bing Xiong,^d Shangcheng Xu,^d Hao Hu,^{a,b,c} Yupeng Xiong,^{a,b,c}
Yuepeng Yan,^d Chunyang Du,^{a,b,c} Wenxiang Peng,^{a,b,c} and
Chaoliang Guan^{a,b,c,*}

^aNational University of Defense Technology, College of Intelligent Science, Changsha, China

^bNational University of Defense Technology, Laboratory of Science and Technology on Integrated Logistics Support, Changsha, China

^cHu'Nan Key Laboratory of Ultra-Precision Machining Technology, Changsha, China

^dNational University of Defense Technology, College of Aerospace Science and Engineering, Changsha, China

Abstract. To realize the quasi-quantitative Schlieren measurement of the shock train structure across the cylindrical isolator in the supersonic flow field, based on the theory of Schlieren measurement and light transmission, we propose the design scheme of conformal windows and discuss the machining feasibility with the window's parameters. The relationship between the Schlieren imaging effect, the deflection of parallel light in the Schlieren apparatus, and the conformal optical window aberrations was researched, putting forward the optical simulation model of the conformal optical windows and the quasi-quantitative Schlieren measurement. Moreover, considering the actual wind tunnel test conditions, under the speed of Mach 2 at the isolator's inlet, the distortion brought by conformal optical windows in the Schlieren observation region was simulated by the computational fluid dynamics method. Finally, the image correction algorithm for the distorted picture caused by the conformal windows was presented, and the quasi-quantitative Schlieren measurement through the conformal optical window pair was conducted for the experimental verification. The results reveal the quasi-quantitative Schlieren measurement effect across the high-precision conformal optical window pair of the cylindrical isolator, providing guidance on maintaining the balance between the manufacturing feasibility and the observation performance of conformal windows. © The Authors. Published by SPIE under a Creative Commons Attribution 4.0 International License. Distribution or reproduction of this work in whole or in part requires full attribution of the original publication, including its DOI. [DOI: [10.1117/1.OE.62.3.035107](https://doi.org/10.1117/1.OE.62.3.035107)]

Keywords: optical imaging; conformal window; cylindrical isolator; Schlieren measurement; computational fluid dynamics simulation.

Paper 20221139G received Oct. 9, 2022; accepted for publication Mar. 9, 2023; published online Mar. 29, 2023.

1 Introduction

As the development of the scramjet technique holds great promise for hypersonic propulsion,¹ the study of the internal flow field structure through ducts becomes a hot research focus. The scramjet consists of the following parts: the inlet, the isolator, the combustion chamber, and the exhaust nozzle.² The scramjet isolator, attracting extensive attention,³ plays a critical role in the connection with the inlet and the combustion by providing compression of the upstream flow and avoiding the disturbance of the backpressure from the downstream.⁴

The concept of the isolator, an additional piece of pipe between the inlet and combustion chamber, was first put forward by Billig et al. in 1972.⁵ Since then, the mainstream research configuration of the isolator has concentrated on a rectangular and cylindrical duct with a

*Address all correspondence to Chaoliang Guan, gchl_nudt@163.com

constant section or microexpanded section. Moreover, the dominant measurement methods of the flow field structure in the isolator include traditional methods (high-frequency pressure gages, thermocouple measurement) and non-contact measurement methods (background oriented Schlieren,⁶ nano-based planar laser scattering,⁷ and Schlieren imaging^{8,9}).

Among the numerous optical measurement methods, the Schlieren imaging measurement is considered the most traditional and qualitative method, which captures the changing of the light intensity by the high-speed camera for the recording of the high-frequency characteristics and the wave structure in the duct. The Schlieren measurement reflects the three-dimensional density distribution information along the optical path on the two-dimensional Schlieren photographs by recording the deflection of the actual light through the internal flow field. For the purpose of the high-precision or even quasi-quantitative Schlieren measurement, the angle of light deflection needs to be recorded accurately on the basis of keeping the emerging wavefront of initial parallel light near zero through the optical window pair.¹⁰ The quasi-quantitative Schlieren measurement not only puts forward high precision requirements for the manufacturing and assembly of the Schlieren mirrors or lenses but also has high quality demands of the Schlieren windows. If the optical windows cannot meet the requirements of high precision, the aberration brought by the optical windows destroys the uniformity of the Schlieren image, which only supports the qualitative recording of the severe flow field variation.⁸

Compared to the rectangular isolator, the cylindrical isolator has shorter shock train length and a stronger ability to withstand back pressure for the performance improvement of the scramjets. Meanwhile, the cylindrical isolator can realize the connection with a cylindrical combustion chamber, which is superior to a rectangular combustion chamber in the fields of the wetted surface area, the structural weight, and the control of hypersonic corner flows.¹¹ Currently, high-precision Schlieren measurements across the pipe mainly focus on the rectangular duct¹² installed with the high-quality plane parallel windows in a mature manufacturing route. However, as for the cylindrical isolator whose inner surface is cylinder, the parallel light deflects when it passes through the pipe, which poses a great challenge to the Schlieren measurement. Until now, the mainstream approach for the Schlieren windows correction has been divided into two schemes: the separate element scheme¹³ and integrated element scheme.¹⁴ The second plan simplifies the system structure by decreasing the number of optical components and reducing the difficulty of the system alignment but increases the difficulty of optical window processing. In the field of quasi-quantitative Schlieren measurement using the integrated scheme through the conformal optical windows, a model of the corresponding relationships among the optical window design, the machining accuracy requirements, and the Schlieren imaging effect has not been established.

As the critical component for quasi-quantitative Schlieren measurements through cylindrical isolators, the conformal optical windows become the core research focus of this paper. The content of this paper revolves around optical design, optical simulation, fluid-structure interaction simulation, and Schlieren measurement experiments. The core part is to explore the influence of the design parameters and processing errors of conformal optical windows on quasi-quantitative Schlieren measurements in wind tunnel tests, which could finally provide specific guidance for the applications of conformal optical windows. The main content of this paper includes the following parts. Based on the theory of Schlieren imaging measurement, the first part presents the optical design model of conformal windows. The second part establishes the optical simulation model of the quasi-quantitative Schlieren measurement and shows the Schlieren measurement effect and range with different window aberrations. The third section describes the fluid-structure interaction simulation result with optical window distortion under actual wind tunnel conditions. The fourth part addresses the image correction algorithm of conformal optical windows. The fifth part displays the quasi-quantitative Schlieren measurement experiment through the high-precision conformal optical window pair. Finally, the conclusion is given at the end of the article.

2 Schlieren Imaging Theory and Conformal Optical Window Design

2.1 Schlieren Imaging Theory

The air is transparent in the invisible refractive phenomenon. When parallel rays pass through the test region with the medium in Fig. 1(a), they refract or bend because of optical inhomogeneities.

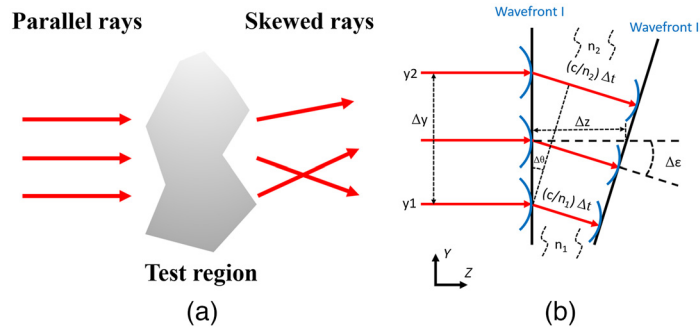


Fig. 1 Description of light deflection phenomenon through inhomogeneous medium: (a) the deflection of the parallel rays passing through the test region and (b) the simplified physical model of the refractive light beam based on refractive index gradient on the y direction.

According to Huygens' Principle, each point on the wavefront becomes a new source of the spherical wavelet. The deflection angle of the refracted light rays can be expressed as the integration of the refractive-index gradient through the beam path. Moreover, depending on the Gladstone–Dale formula, there is an apparent linear relationship between the gases' refractive index n and density ρ . To simplify the physical phenomenon, a model with the negative vertical refractive-index gradient ($dn/dy < 0$) was constructed,⁸ as shown in Fig. 1(b). It can be demonstrated that the parallel rays propagate through wavefront I and wavefront II in turn within the same differential time Δt when they pass through the Schlieren object. Moreover, each point on the wavefront I traverses a different distance Δz with a differential angle $\Delta \epsilon$ by virtue of the different refraction n along the y direction. Consequently, the wavefront II tilts clockwise toward the higher-refraction-index region, which has higher density ($n_1 > n_2$).

The integration result of the deflection angle along the z direction is given by the following equation:⁸

$$\epsilon_y = \frac{1}{n} \int \frac{\partial n}{\partial y} dz, \tag{1}$$

where the angle ϵ_y can accurately reflect the distribution of refraction index n along the light path as well as the distribution of density ρ on account of the Gladstone-Dale formula.

After bringing the physical model of the turbulent flow mentioned above to the Schlieren apparatus, the deflection of the light caused by the inhomogeneous test region needs to be recorded exactly for the purpose of the quasi-quantitative Schlieren measurement. As shown in Fig. 2, the change of the light brightness ΔI on the camera and the position offset of the ray Δa on the plane of the knife-edge are affected at the same level by virtue of the deflection angle ϵ_y of the parallel light. The integral result of the deflection angle ϵ_y along the test region can be simplified to the angular deflection only through one plane P1, which is in the middle of

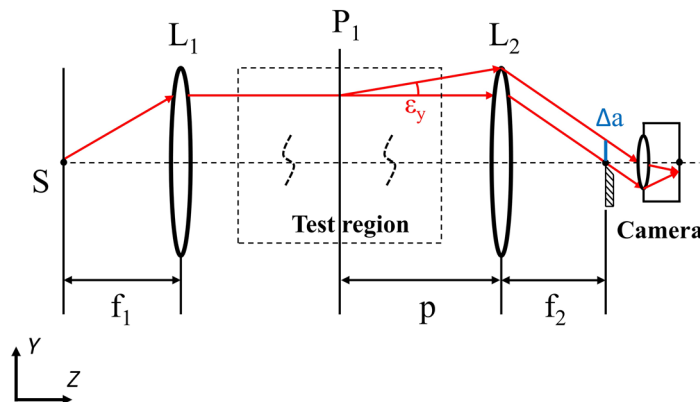


Fig. 2 Deflection of the parallel light in the Schlieren apparatus.

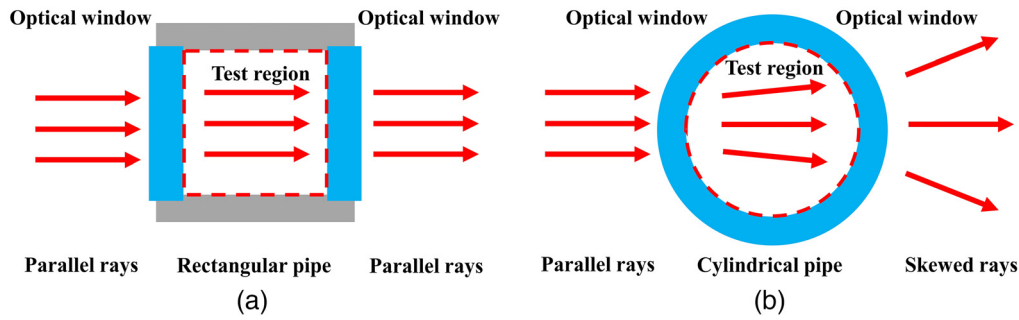


Fig. 3 Schematic diagram of the parallel rays through (a) rectangular pipe and (b) cylindrical pipe in the Schlieren apparatus.

the test region. Combined with the Eq. (1), the proportion of the irradiance change on the camera relative to the original irradiance value can be derived as in Eq. (2).⁸ As long as the change value of the irradiance can be recorded precisely, the corresponding integral of the refractive-index can be calculated accurately

$$\frac{\Delta I}{I} = \frac{\Delta a}{a} = \frac{f_2 \varepsilon_y}{a} = \frac{f_2}{a} \cdot \frac{1}{n} \int \frac{\partial n}{\partial y} dz. \quad (2)$$

For the purpose of the quasi-quantitative Schlieren measurement through the isolator, the primary principle is to ensure that the shape of the inner flow channel would not be destroyed during the wind tunnel operation process and Schlieren measurement process. The plane optical windows can fit the inner flow channel shape of the rectangular isolator well. When the plane windows are applied to the cylindrical isolator whose bilateral walls are changed to flat shapes, all the flow field characteristics in the original cylindrical flow channel are destroyed, resulting in inaccurate measurement results. Then, the corresponding optical path of the parallel rays needs to be maintained. When the plane windows are applied to the duct with a rectangular cross section in Fig. 3(a), the channel of the parallel light through the pipe has not been damaged. Correspondingly, in contrast to the cylindrical duct with the outer concentric cylindrical surfaces, the incident parallel rays skew after leaving the other side of the pipe in Fig. 3(b). The deflected rays caused by the optical windows destroy the uniformity of the initial picture background taken by the Schlieren camera, and the valuable information recorded by the parallel rays through the test region are submerged in the complicated background. Moreover, the unidirectional Schlieren measurement range whose direction is perpendicular to the knife-edge tends to become saturated owing to the initial poor Schlieren picture background. As a consequence, this poses a great challenge for the quasi-quantitative Schlieren measurement through the cylindrical pipe.

2.2 Optical Design of Conformal Optical Windows

In consideration of the light deflection brought by the outer concentric cylindrical surface above, the feasible design of the conformal optical windows needs to obey the principle that takes the transmitted wavefront errors of the parallel light through the windows as the optimization objective.¹⁵ As shown in the optical design diagram of the silica conformal window in Fig. 4, the radius R of the surface S_1 of the internal duct was set as 50 mm, and the relevant outer surface S_2 and the thickness of the window L were applied together to the correction of the transmitted wavefront errors. As the diameter D_1 of the incident light varies, the corresponding diameter D_2 of the emergent light changes.

On the strength of the determinate inner surface structure, the outer surface takes sixth-order aspheric cylinder for the error correction by the damped least-square method in the optical design software, and the final wavefront error (peak-to-valley value, PV value) of transmitted light is ΔW . The sixth aspheric cylinder surface sag is given by the following equation:

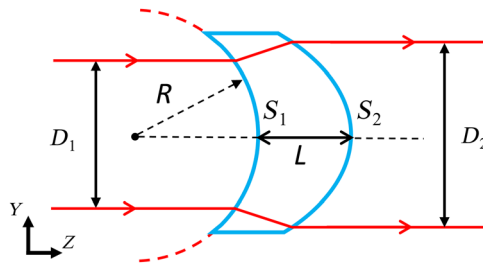


Fig. 4 Optical design model of the conformal window.

Table 1 Multiparameter influence on the asphericity of the outer surfaces.

Number	D_1 (mm)	L (mm)	ΔW (λ^a)	Asphericity (mm)
1	50	10	0.0003	0.0039
2	50	30	0.0006	0.0119
3	50	50	0.0003	0.0199
4	30	30	0.0000	0.0012
5	70	30	0.0349	0.0674

^a $\lambda = 632.8$ nm

$$Z = \frac{cY^2}{1 + \sqrt{1 - (1 + k)c^2Y^2}} + A_4Y^4 + A_6Y^6, \tag{3}$$

where c represents the curvature, k is the conic constant, and A_4 and A_6 are the coefficients of aspheric cylinder. The selected operating wavelength of the optical system is 632.8 nm.

Based on the aspheric cylinder equation of the outer surface S_2 with the same length along the generating line, the discussion of the machining difficulty can focus on the asphericity of the transversal curve. Compared with multiple parameters to describe the aspheric cylinder equation in Eq. (3), the asphericity value can describe the machining difficulty more intuitively. There are many representation methods of the asphericity. In this study, taking the vertex and the endpoints of the outer surface within the optical region D_2 for fitting the circle, the corresponding maximum deviation value between the designed transversal curve of the outer surface and the fitting circle could be calculated as the asphericity. During the machining process, the larger the asphericity value is, the more difficult it is to process the outer surface based on the more amount of material removal from the best-fit cylindrical surface. The design and simulation results based on the different structure parameters are given in Table 1.

From the simulation results in Table 1, it can be seen that when the diameter D_1 of the incident beam is kept constant, as the thickness L increases, the asphericity value rises. Moreover, when the thickness L is fixed, the diameter D_1 of the incident beam rises at the expense of the increasing of the outer surface's asphericity. Hence, when we aim at a certain structure of the isolator duct, the larger diameter of the incident beam can obtain more information within the larger observation region by the Schlieren measurement, and the thicker windows can acquire stronger impact resistance when faced with the more extreme conditions in the wind tunnel experiment. However, a larger diameter of incident light and thicker window can result in greater manufacturing difficulty with larger asphericity, so the overall design structure of the conformal optical windows needs to be considered comprehensively.

3 Quasi-Quantitative Schlieren Imaging Analysis with Conformal Optical Window Aberration

For the purpose of the high-precision or quasi-quantitative Schlieren optical measurement, the subtle changes in density through the flow field need to be detected accurately by the Schlieren

Table 2 Conformal optical window parameters.

Material	Surface	Type	Radius/mm	Thickness/mm	Conic	Aspheric cylinder orders
Silica	S ₁	Cylinder	-50	30	/	/
	S ₂	Aspheric cylinder	-59.409991	/	-0.099681	Fourth order and sixth order

apparatus. First, the subtle density changes correspond to the slight variation of irradiance on the Schlieren camera, which means a uniform and bright picture irradiance background cut by the knife edge in the initial stage is a critical factor for the high-precision Schlieren measurement. This guarantees that weak density changes are not covered by the irradiance background. Second, to make sure the subtle density changes could be quantitatively measured, the corresponding deflected angle of the parallel light needs to be measured accurately, which can deduce the integral of the refractive index along the light path.

Therefore, from the perspective of the uniformity of the observation background and the high-precision measurement of the deflection angle from the parallel rays, this section analyzes the quasi-quantitative Schlieren measurement in combination with the conformal optical window aberrations.

To implement the corresponding simulation above, we need to construct the numerical simulation model based on the designed conformal window structure. From the analysis result at the end of Sec. 2.2, the bigger incident beam diameter and thicker conformal window corresponds to the bigger asphericity value, which are unfavorable for processing. The conformal window with bigger incident beam diameter corresponds to the more observational information from the flow field in the pipe, and the thicker conformal window corresponds to the better bearing strength, which can withstand more severe experimental conditions. Under the comprehensive consideration, we chose the median values of the incident beam diameter and the window's thickness in Table 1, which is the group of Number 2. The corresponding parameters are displayed in Table 2.

3.1 Schlieren Imaging Background with Conformal Optical Window Aberration

For the simulation of the imaging effect in the Schlieren apparatus, the most popular Schlieren apparatus with the z-type configuration was used for the numerical simulation in this part, which has the universality of multiple wavelengths and a lower cost than the transmission Schlieren system.

The ray tracing method in combination with the optical design software and programming algorithms was used in the numerical simulation of the z-type Schlieren imaging system in Fig. 5. The rectangular light source S images at the slit through the condenser form a uniform

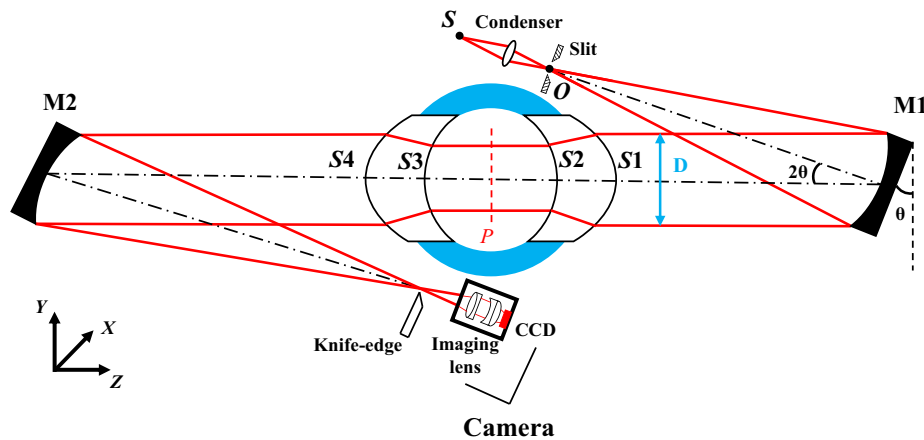


Fig. 5 Z-type Schlieren imaging system with conformal optical windows.

spot O , with both the length and width being 5 mm. The light spot O reaches the collimating mirror $M1$, bilateral conformal optical windows, and converging mirror $M2$ in turn. Then, the spot i focuses on the knife-edge plane and is cut by the knife-edge at a self-defined rate. Finally, the rays imaging on the charge coupled device (CCD) can be seen through the imaging lens group in the camera. In the simulated structure, the $M1$ and $M2$ are spherical mirrors with the focal length of 2 m and a diameter D of the used spot size of 60 mm, which means that the F number of the system is much larger than 10,¹⁶ and the parameters of the Schlieren system meet the usage requirements compared with the aspherical mirrors.

In consideration of the regular circular structures of the reflector $M1$ and $M2$ in the z -type Schlieren apparatus in Fig. 5, the actual passage area of the parallel light during Schlieren measurements is limited in a circular region. Meanwhile, during the simulations of the transmitted wavefront errors in Sec. 2.2, the incident parallel beam was set as a circular spot. Hence, in order to explore the relationship between window aberrations and Schlieren imaging effects, the optical region in this study was set as the circular aperture within the conformal optical windows. Furthermore, the optical window aberrations within the circular area can be fitted by Zernike polynomials that have continuous orthogonality over the unit circle domain and can correspond to the low-order aberrations clearly. In the simulation of the parallel light path through the conformal optical window pair, the parallel rays from the light source pass through the surface $S1$, $S2$, $S3$, and $S4$, successively. The number of virtual rays from the light source was set as 6561, and the window aberration was applied to the $S4$, which contains the common low order aberrations of piston, tilt, power, astigmatism, and coma (the lowest eight terms of Zernike standard polynomials). In each aberration on surface $S4$ mentioned above, the transmitted wavefront error (PV value) through bilateral optical windows was controlled to 10λ ($\lambda = 632.8$ nm). The final imaging effects of simulation, including the normalized grayscale image and corresponding pseudocolor image, are shown in Figs. 6(a)–6(j).

The color threshold range of the grayscale images in Figs. 6(a)–6(j) is from 0 to 255, and Fig. 6(a) demonstrates the Schlieren imaging effect through the conformal optical windows without aberration, whose color-order value is 255 within the whole observation area. The grayscale image in Fig. 6(a) is the normalized base image for the following grayscale picture.

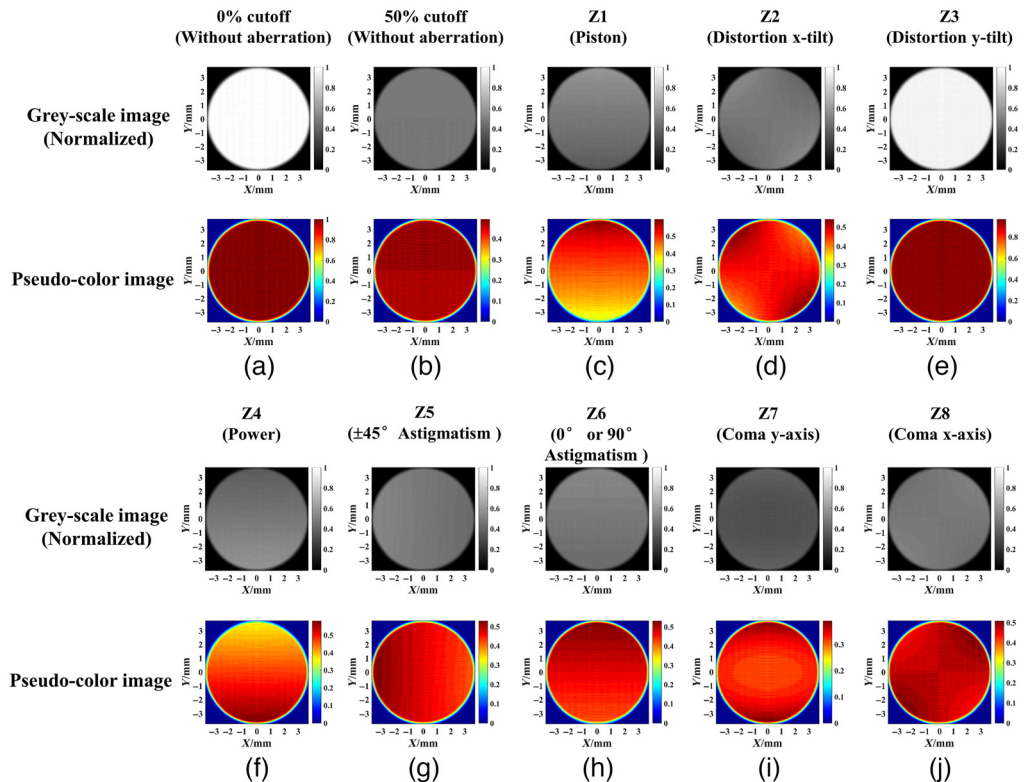


Fig. 6 (a)–(j) Imaging effects of different kinds of aberrations in the Schlieren imaging system.

The grayscale image in Fig. 6(b) shows the Schlieren imaging result at a cutoff rate of 50% by the knife edge, and Figs. 6(c)–6(j) displays the Schlieren imaging picture at a 50% cutoff with the different window aberrations mentioned before. The pseudocolor images are normalized on the respective grayscale image to show the uniformity of the image distribution.

On the basis of the theoretical analysis in Sec. 2.1, the uniformity of the imaging background with no flow field disturbance condition is a crucial factor for the quasi-quantitative Schlieren optical measurement. Under the transmitted wavefront error value of 10λ brought by the aberration on the surface S4, corresponding to the background uniformity of the 50% cutoff in Fig. 6(b), Fig. 6(e) with tilt distortion on the y-axis shows the best uniformity among the results of the Schlieren imaging background of different aberrations. By contrast, there is $>25\%$ difference between the normalized maximum gray value and the minimum gray value in the pseudocolor image of the rest aberrations on surface S4, which reflects enormous destruction to the quasi-quantitative Schlieren measurement. By comparing the Fig. 6(b) with Fig. 6(c) and Figs. 6(d)–6(j) separately, when the wavefront error of each aberration reduces to the value in Fig. 6(b), which is close to zero, the surface shape error of each kind of aberration on the outer surface will decrease to zero and the corresponding Schlieren imaging background will change to an uniform pattern in Fig. 6(b). The Schlieren imaging pattern is actually a reflection of the degree of parallel light deflection. If the surface shape error of the outer surface increases, which means the transmitted wavefront error through the conformal window rises, the corresponding deflection angle of the parallel rays in the Schlieren apparatus will increase, resulting in an increase of contrast in the light and dark regions within an uneven image background. Hence, the high-precision and even quasi-quantitative Schlieren measurements need a high-quality Schlieren window with small transmitted wavefront error with good uniformity of the Schlieren imaging background.

3.2 Deflection of Parallel Rays with Conformal Optical Window Aberration

For the purpose of the quasi-quantitative Schlieren measurement, there not only needs to exist a uniform imaging background but also the accurate recording of the deflection angle in the case of flow field disturbance. Compared to the simple geometric model of the light refraction through the plane window in Fig. 7(a), which displays the clear relationship of the equal deflection angle value between the incident and emergent rays ($\theta = \theta'$), there is a complex relationship between the incident angles and the emergent angles through the conformal windows ($\theta \neq \theta'$) in Fig. 7(b), especially attaching with the window aberrations. Moreover, only the emergent angle value could be finally detected and recorded by the Schlieren measurement, according to the optical model in Fig. 2.

According to the theory model of the Schlieren measurement in Sec. 2.1, the light deflection through the internal flow field could center on the light deflection on the object plane S in the middle of the duct. The parameters of the bilateral conformal optical window without aberration are shown in Table 2. For the simulations of the deflection angles of the parallel rays through the distorted conformal optical window with different kinds of aberrations. The aberrations of the typical low-order aberrations represented by the lowest eight terms of Zernike standard

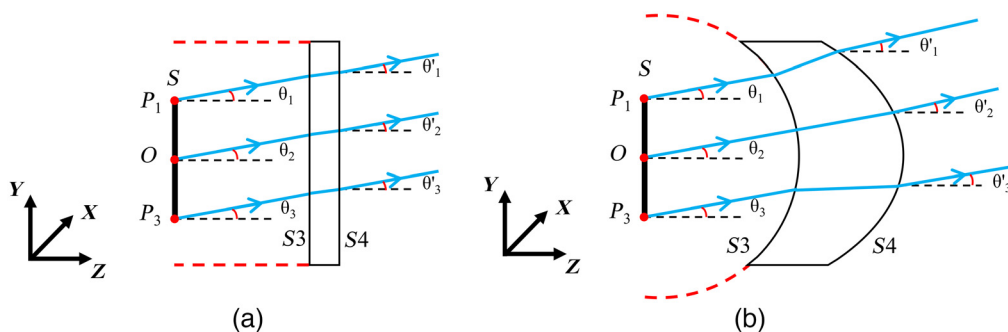


Fig. 7 Two-dimensional model of light deflection through (a) the plane window and (b) the conformal window.

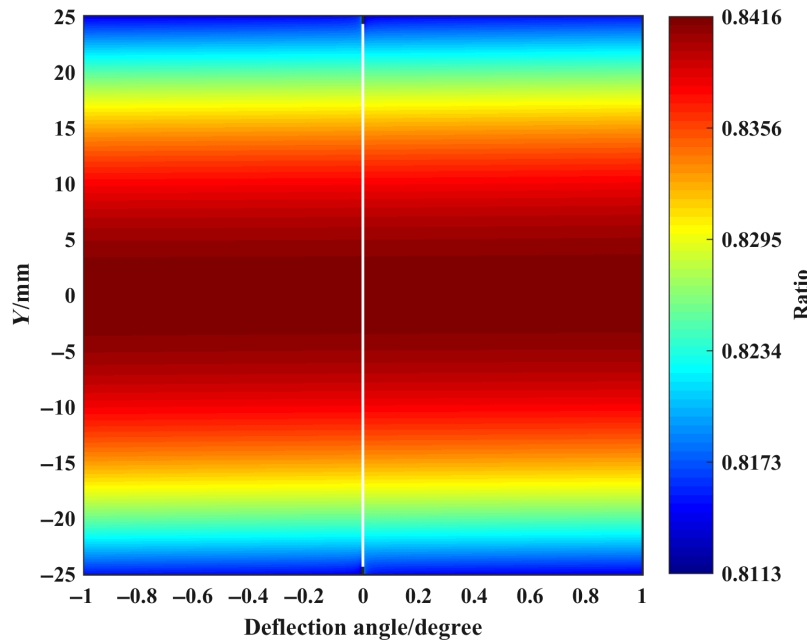


Fig. 8 Ratio of the emergent angle θ' to the deflection angle θ along the Y direction.

polynomials are applied in this part, which similarly correspond to the piston, distortion x -tilt, distortion y -tilt, power, ± 45 deg astigmatism, 0 deg or 90 deg astigmatism, coma y -axis, and coma x -axis in Sec. 3.1. The aberrations of the lowest eight terms of Zernike standard polynomials are added on the outer surface S4 in Fig. 7(b), whose transmitted wavefront error (PV value) is 1λ through the unilateral optical window. The corresponding numerical relationship between the deflection angle θ from the object plane S and the emergent angle θ' needs to be established. As shown in Fig. 7, the rectangular observation region of the object plane S in the X direction and Y direction is 100 and 50 mm, respectively. The point O is the midpoint of $\overline{P_1P_3}$ and the geometric center of the object plane S.

On the basis of the initial conformal optical window model without aberration whose inner surface and outer surface are cylinder and aspheric cylinder respectively, the corresponding ratio of the emergent angle θ' to the deflection angle θ along the Y direction is shown in Fig. 8. The value of the deflection angle θ in Fig. 8 ranges from -1 deg to 1 deg, and the maximum value and minimum value of the ratio are 0.841 and 0.811, respectively. The difference between the maximum and minimum is 0.03, which accounts for the 3.6% to the maximum value 0.841. On account of the theoretical analysis of the sensitivity by Goldstein,¹⁷ the variation proportion of the deflection angle under 5% is regarded as the indistinguishable result in the Schlieren measurement. The simulation variation value of 3.6% is within this scope, and the calculated mean proportion value in the whole observation area is 0.832. From the simulation results in Fig. 8, there is a conjugation relationship between the emergent and incident rays leading to the nearly constant ratio of the light deflection angle at the same y value. Due to the set evaluation factor of the evenly distributed incident parallel rays within the whole observation region during the optical design process, the corresponding change rate of the final transmitted wavefront error has the gradual reduction tendency from the center to the upper and lower region. Hence, Fig. 8 shows the symmetry along the y direction at the same deflection angle of the incident ray, which reveals a slight difference of the light correction ability corresponding to the ratio of the deflection angles between the central area and the surrounding area. When the deflection angle of the incident parallel rays is zero, the corresponding ratio of the deflection angle is meaningless due to the ratio's denominator of zero. Hence, there is a white line in the middle of the Fig. 8 forming a gap of the positive and negative deflection angles of the incident parallel rays.

However, when the aberrations are appended to the outer surface S4 of the conformal optical windows, the corresponding ratio value of the emergent angle θ' and the deflection angle θ change dramatically. Therefore, the actual deflection angle value in the duct could not be

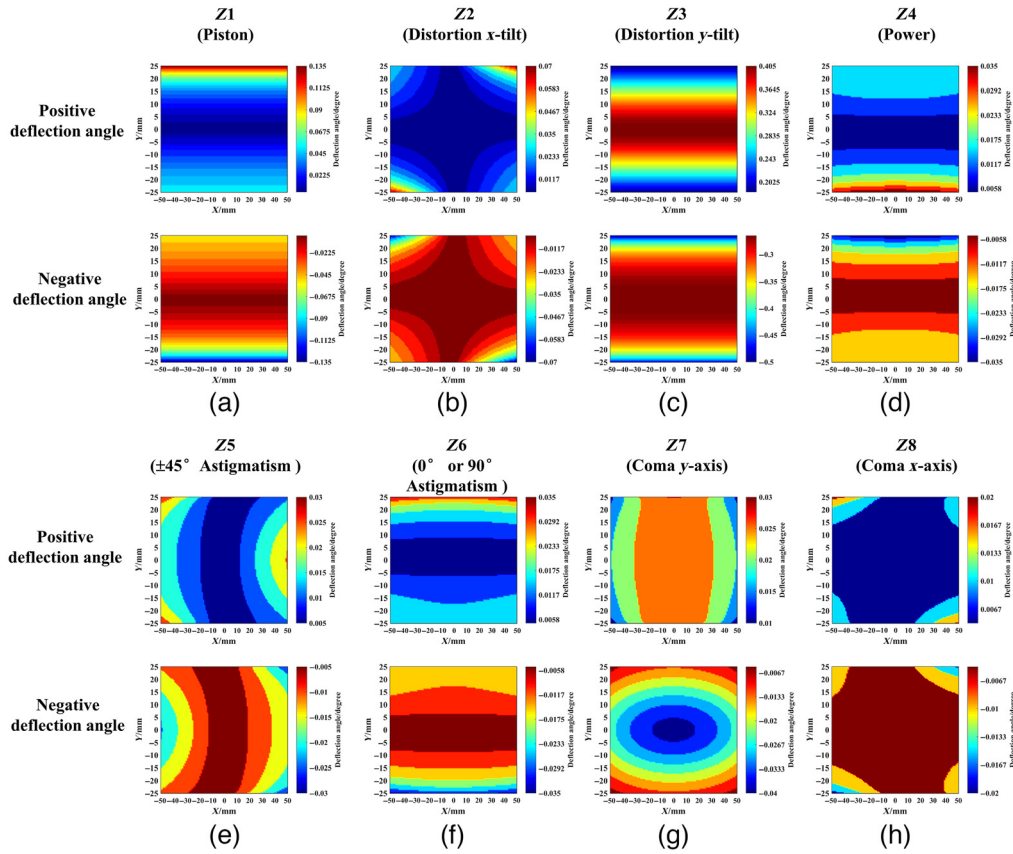


Fig. 9 (a)–(h) Acceptable minimum absolute deflection angle with a positive and negative deflection angle in the whole observation area with different window aberrations.

calculated based on the determined ratio value and the measurable emergent angle value. In order to achieve the quasi-quantitative measurement in the Schlieren apparatus, the simulations in this part set the indistinguishable ratio range to 5% (the corresponding ratio value is 0.04), which means that the applicable ratio scope between the emergent angles and deflection angles are 0.832 ± 0.04 .

From the results in the process of the numerical simulation, within the given ratio scope of 0.832 ± 0.04 , as the absolute values of the deflection angles increase, the corresponding ratio value returns to the given ratio scope gradually from the distortion value for any point on the object plane S. However, when the absolute values of the deflection angles are too small, the corresponding ratio value generates numerical mutations and exceeds the threshold of the applicable ratio scope. This means that the window aberrations produce a large distortion of the ratio value when the light rays deflect at a small angle through the flow field region, which leads to great destruction to the quasi-quantitative Schlieren measurement. Hence, when the absolute values of no matter positive or negative deflection angles are beyond the minimum absolute deflection angles, the corresponding ratio values are maintained in the given ratio scope. Based on this change rule of the deflection angles in the simulation model, as each aberration is added to the surface S4, the calculated minimum absolute deflection angles of the positive and negative angles are shown in Fig. 9, which shows the effects of the different widow aberrations on the deflection angles of the quasi-quantitative Schlieren measurement within the whole object plane S.

Figure 9 shows that as the window aberrations are added to the outer surfaces, the minimum absolute deflection angles in the range of quasi-quantitative measurement fluctuate. Meanwhile, the corresponding comparison diagram of maximum value of minimum acceptable absolute deflection angle in the whole observation region corresponding to the aberrations above is shown in Fig. 10. The calculated absolute deflection angles in Figs. 9(d)–9(h) are relatively small, which corresponds to the aberrations of Z4 (power), Z5 (± 45 deg astigmatism), Z6 (0 deg

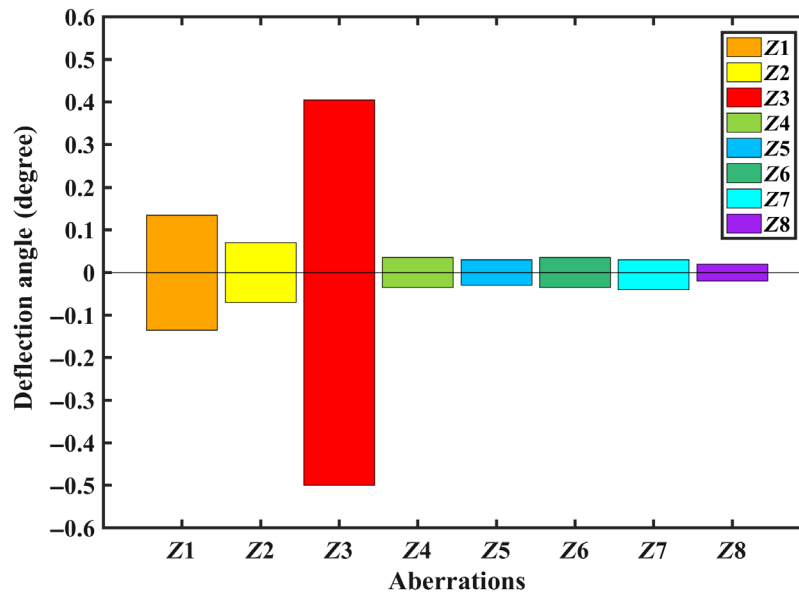


Fig. 10 Comparison diagram of maximum value of minimum acceptable absolute deflection angle of different aberrations.

or 90 deg astigmatism), Z7 (coma y -axis), and Z8 (coma x -axis) in Fig. 10. These five kinds of aberrations have the least impact on the quasi-quantitative Schlieren measurement. By contrast, the aberrations of the Z1 (piston), Z2 (distortions x -tilt), and Z3 (distortions y -tilt) in Figs. 9(a)–9(c) correspond to the bigger absolute deflection angles among the various aberrations, which causes destruction to the quasi-quantitative Schlieren measurement. In particular, compared with the uniformity analysis of the Schlieren background in Sec. 3.1, although the aberration of Z3 (distortion y -tilt) in Fig. 6(e) has excellent uniformity of the imaging background, it destroys the feasibility of the quasi-quantitative Schlieren measurement in the range of the small absolute deflection angles in Fig. 9(c), which corresponds to the biggest value of minimum absolute deflection angle in Fig. 10. Regardless of the type of aberration there is, the quasi-quantitative Schlieren measurement can be realized beyond the absolute deflection angles with the different intensity changes of the flow field.

In conclusion, the analysis results above can put forward some instructive suggestions on the quasi-quantitative Schlieren measurement with the conformal optical windows in the link of the manufacturing. First, from the perspective of the initial Schlieren imaging background, the higher machining accuracy for the eliminating of the different manufacturing aberrations on the optical surfaces, the smaller transmitted wavefront error, which except for the aberration of the y -tilt distortion, could achieve a more uniform Schlieren background. Second, from the perspective of the quasi-quantitative measurement of the deflection angles, the aberrations of the piston, x -tilt distortion, and especially the y -tilt distortion of the conformal windows should be vigorously eliminated in the manufacturing link. If the window processing aberrations cannot be well controlled, the corresponding conformal optical windows can only be applied to the flow field with acute change in the field of quasi-quantitative or even qualitative Schlieren imaging measurement.

4 Fluid-Structure Interaction Analysis of Conformal Optical Windows

Aiming at the actual usage of the conformal optical windows in the cylindrical isolator, the windows aberrations caused by the wind tunnel operation conditions would affect the quasi-quantitative Schlieren measurement through the pipe. This part would carry out simulation of the aberrations of the conformal windows by the fluid-structure interaction analysis.

The common materials of the Schlieren optical windows include acrylic¹⁸ and silica.¹³ As shown in Fig. 11, the incoming flow travels through the Mach 2 nozzle and forms the supersonic flow field. The cylindrical isolator, whose diameter D is 100 mm and whose length L_0 is

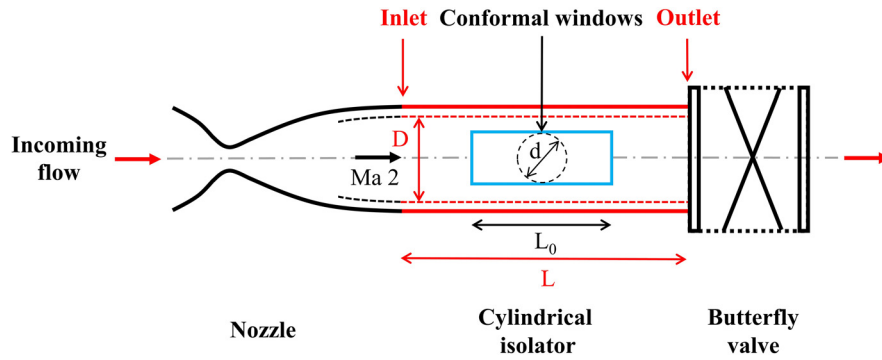


Fig. 11 Schematic configuration of wind tunnel test with the cylindrical isolator.

200 mm, is installed between the nozzle and the butterfly valve, whereas the conformal optical window pair, whose inner diameter is 100 mm and whose thickness is 30 mm, is mounted on each side of the isolator. The diameter d of the optical region in the Schlieren measurement through the outer surface of the conformal windows is 60 mm. In the static environment, as the conformal window structure shown in Fig. 4, the corresponding transmitted wavefront errors (PV value) corrected by the outer aspheric cylinder are 0.0001 and 0.0009λ of the acrylic and silica materials, respectively.

When the wind tunnel is in operation, the corresponding window distortion caused by the actual conditions could be simulated using the fluid-structure interaction method. In the simulation part, the computational fluid dynamics simulation was conducted for the isolator flow field. The finite volume method was used to discretize the Reynolds averaged compressible Navier-Stokes equation of 3D. The turbulence model of shear stress transport (SST) $k - \omega$ was applied in the simulation of the shock train. When we set the incoming flow of the inlet as an ideal gas with the pressure far-field condition, the gauge pressure of the incoming flow is 12.95 kPa, and the Mach number is 2. A steady back pressure of 51.8 kPa is forced by the butterfly valve at the location of the outlet to form the shock train within the observation area of the conformal windows. The corresponding grid distribution of the cross profile of the flow field with the mesh encryption on the wall is shown in Fig. 12(a) and the total number of the structured grid cells of the flow is 289,365. The convergence criteria for the simulation calculation of the shock train is the calculated residual value less than 10^{-3} , and the mass flow rate between the inlet and outlet cross section is less than 10^{-4} kg/s. In the final steady-state calculation result, the cross section of the static pressure distribution in the middle of the isolator is shown in Fig. 12(b).

Appending the steady-state pressure distribution along flow field to the isolator pipe with the conformal windows, the corresponding deformation results are displayed in the Fig. 13.

In view of the differences in the material properties between the silica and acrylic, especially the material variance in Young's modulus values, the deformation of the acrylic conformal

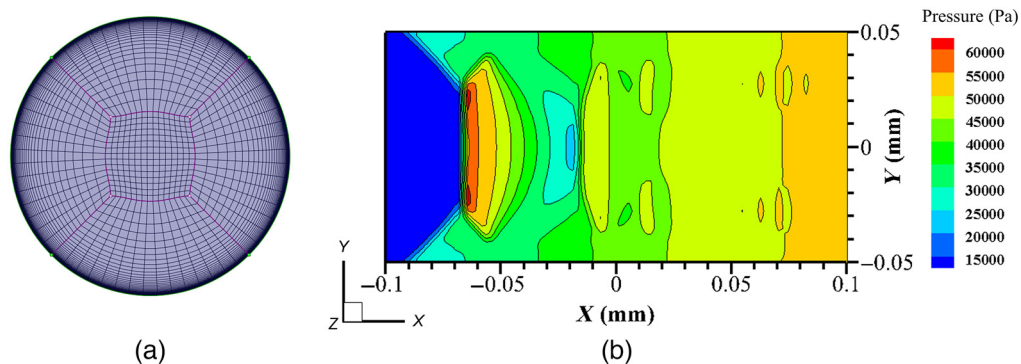


Fig. 12 (a) Grid distribution of the isolator and (b) the distribution of the static pressure of the cross section in the middle of the isolator.

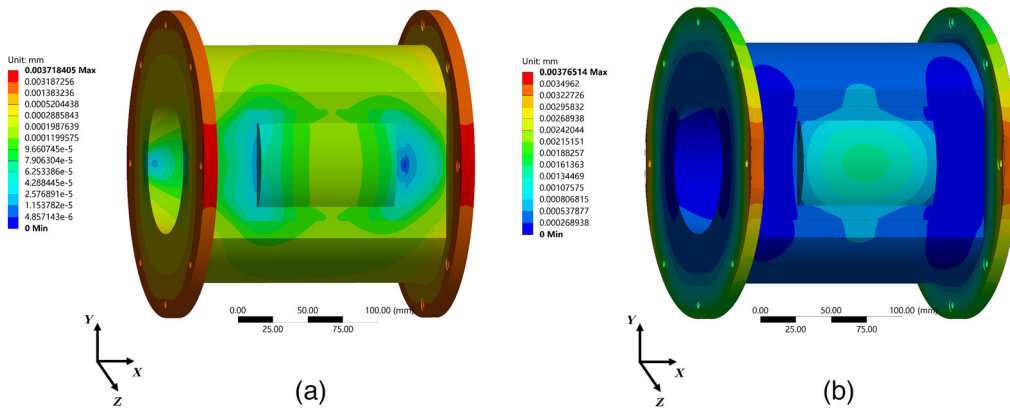


Fig. 13 Deformation results of the isolator pipe with the (a) silica conformal optical windows and (b) acrylic conformal optical windows.

windows is larger than that of the silica windows in Fig. 13. To realize the exact calculation of the transmitted wavefront error through the distorted conformal windows, we fitted the deformation amount of the inner and outer surfaces of the conformal windows by the Zernike polynomial for the quantitative calculation. The corresponding deformation sag values of the inner and outer surfaces of the silica and acrylic windows are shown in Fig. 14.

Bringing the surface-shape error into the optical model of the conformal windows, the corresponding transmitted wavefront error (PV value) of the silica and acrylic conformal windows through bilateral optical windows was calculated as 0.0122 and 0.4361λ , respectively, which means that the transmitted wavefront distortion of the acrylic material is larger.

Combined with the above analysis results in Sec. 3.2 and the degree of the light reflection in the actual shock train structure through the isolator, the transmitted wavefront error of the sub-

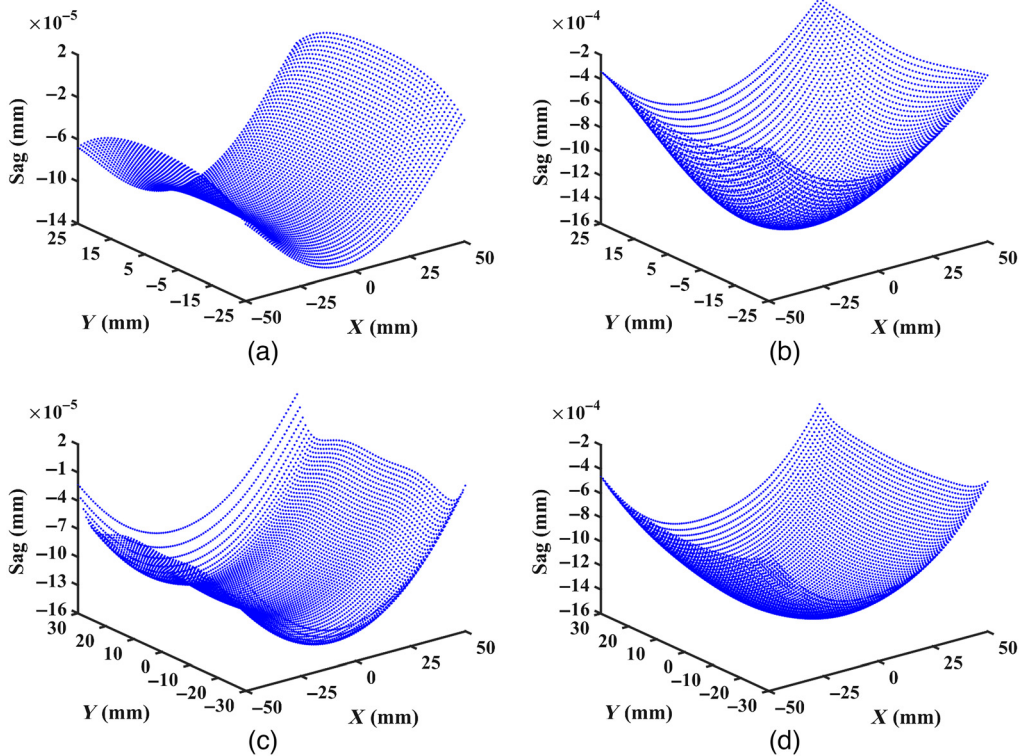


Fig. 14 Deformation sag of the (a) inner and (c) outer surfaces of the silica conformal windows and the (b) inner and (d) outer surfaces of the acrylic conformal windows on the +Z side.

wavelength level would not affect the quasi-quantitative Schlieren measurement in the actual operating condition. The Schlieren measurement through the distorted silica conformal optical windows could achieve clearer measurements and capture more details of the flow field structure than the acrylic windows under the same operating conditions.

5 Schlieren Image Correction of Conformal Optical Windows

In view of the cylinder and aspheric cylinder shape of the inner and outer surfaces of the conformal windows, compared with the parallel plane windows, the Schlieren picture shot by the high-speed camera through the conformal windows would produce a huge distortion, causing damage to the quasi-quantitative Schlieren measurement. For the accurate capture of the flow field information in the isolator, starting from the geometric structure analysis of the conformal optical windows, the Schlieren picture information needs to be corrected.

Based on the optical structure of the silica conformal windows shown in Table 2, the half width of the incident beam r_1 was set to 25 mm and the thickness of the conformal window t_0 was set to 30 mm, which is shown in Fig. 15. At the operating wavelength of 632.8 nm, the corresponding refractive index of the silica n_λ is 1.457, with the transmitted wavefront error (PV value) of 0.0006λ . The marginal ray of the parallel beam starts from point A_1 on the surface S_0 and passes through point A_2 and A_3 on the inner surface S_1 and the outer surface S_2 in turn, respectively. Finally, the emergent parallel ray arrives at the point A_4 on surface S_3 , which corresponds to the outgoing beam half width r_2 .

From the theoretical deduction of the geometric optics in the Ref. 19, setting point O as the origin coordinate $(0, 0)$, the length of OA_2 is r_0 , the fixed window thickness value PQ is t_0 , and the distance of A_2A_3 is t . The derived coordinates of point A_3 are given by the following equation:

$$\begin{aligned} X &= r_0 \cos \theta_1 + t \cos \theta_2 \\ Y &= r_0 \sin \theta_1 + t \sin \theta_2. \end{aligned} \tag{4}$$

Depending on the Snell's law of refraction, the relationship between the angles θ_1 and θ_2 could be obtained through mathematical derivation in the following equation:

$$\sin \theta_1 = n_\lambda \cdot \sin(\theta_1 - \theta_2). \tag{5}$$

On the basis of the Malus law, the optical path differences of any rays between the object plane S_0 and the image plane S_3 are all equal, which is shown in the following equation:

$$t(n_\lambda - \cos \theta_2) = t_0(n_\lambda - 1). \tag{6}$$

The theoretical proportional value of the emergent parallel beam half width r_2 and the incident parallel beam half width r_1 with the change of r_1 could be calculated according to Eqs. (4)–(6). In the optical simulation model of the conformal windows in Table 2, the corresponding ratio value calculation could be calculated using the ray tracing method. Figure 16 displays the theoretical and simulation results of the ratio of r_2/r_1 .

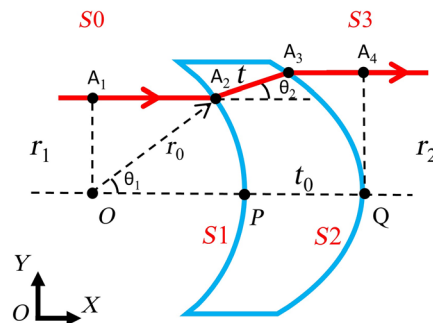


Fig. 15 Two-dimensional structure diagram of the conformal optical window.

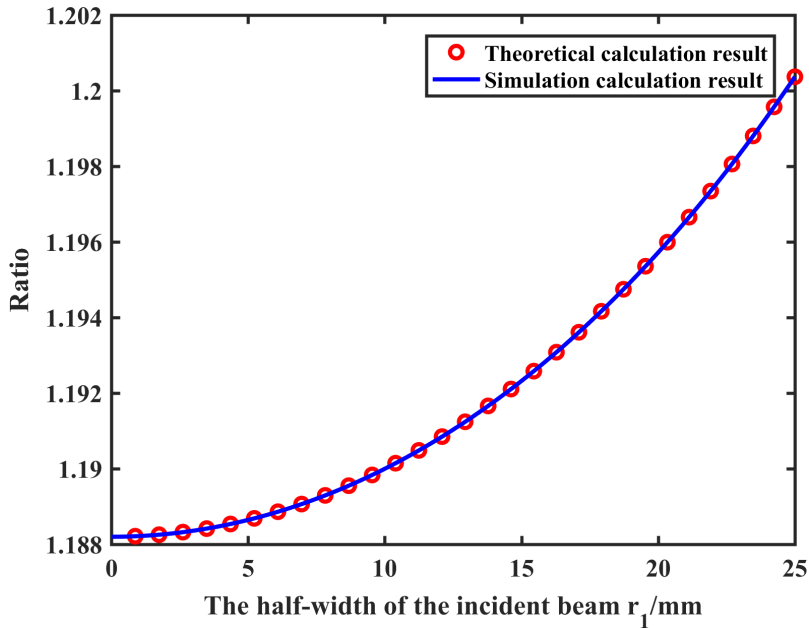


Fig. 16 Ratio value with the change of the half of the incident beam r_1 in theoretical and simulation results.

As shown in Fig. 16, which reveals the consistency of the ratio value in theoretical and simulation results, there exists a nonlinear relationship between the emergent beam half width r_2 and the incident beam half width r_1 . Moreover, as the half width r_1 increases, the corresponding ratio value increases faster. The actual photograph taken by the Schlieren camera only displays the distortion flow field information within the observation region of the outer optical surfaces. However, the true information inside the pipe needs to be recovered with the multiplication of the corresponding proportionality coefficient in Fig. 16, which is a crucial part of the quasi-quantitative Schlieren measurement.

6 Quasi-Quantitative Schlieren Measurement Experiment

According to the above theoretical and simulation analysis, in order to verify the feasibility of quasi-quantitative Schlieren measurement through the conformal optical window pair of the cylindrical isolator, this section describes how we conducted the corresponding Schlieren measurement test. The ready-made cylindrical isolator with the conformal optical windows, which is shown in Fig. 17(a) in the Ref. 20, was used for the experiment, whose interferometric measurement result within the size of 84.89 mm × 46.24 mm is shown in Fig. 17(b). The transmitted wavefront errors through the bilateral optical windows are 12.189 λ (PV value) and 2.658 λ (root-mean-square value).

Based on the self-built z-type Schlieren measurement system in Fig. 18, the rays from the light source pass through the spherical reflector M1, the conformal optical window pair, and spherical reflector M2 in turn. With the rays cut by the knife-edge in the light path, the Schlieren measurement patterns are imaged onto the CCD of the camera (model: A5201MU150, HuaRay Technology Co.). The diameter and the focal length of the mirror M1 and M2 are 150 and 750 mm, respectively.

For the demonstration of the quasi-quantitative Schlieren measurement through the conformal optical windows, the calibration lens (model: PLCX-25.4-5151.0-C) was used in the light path of the Schlieren apparatus. According to the Schlieren measurement experiment setup in the Ref. 21, the thin lens with a long-focal-length could satisfy the relationship in the following equation:

$$\varepsilon \approx \tan \varepsilon = \frac{r}{f_{\text{lens}}}, \tag{7}$$

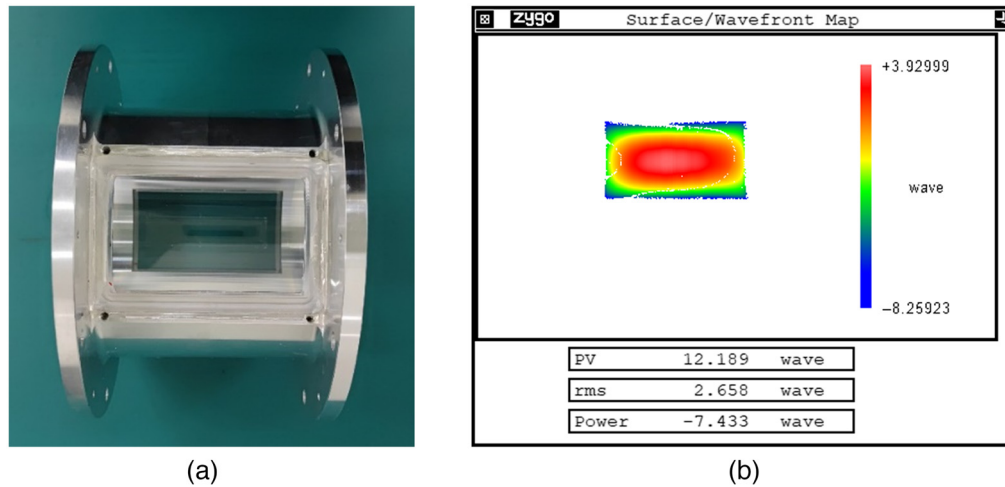


Fig. 17 (a) Cylindrical isolator with conformal optical windows and (b) interferometric measurement result.²⁰

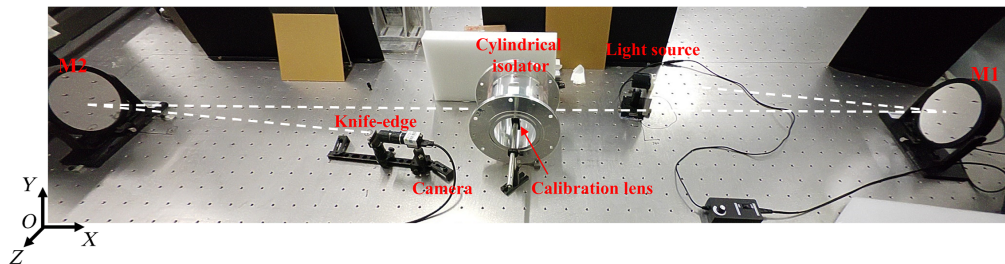


Fig. 18 Z-type Schlieren measurement system.

where ε represents the light deflected angle within the geometric size of the lens, r is the distance between the ray and the geometric center point of the lens, and f_{lens} is the lens's focal length value. The calibration lens's focal length is much larger than its geometric size, which meets the requirements above. Hence, there is a linear ratio relationship between the light deflected angle ε and the distance value r , which was well represented in the Ref. 21.

Taking the frame rate as 100 fps and exposure time as 1/833 s, the original black-and-white photograph with a 50% cutoff of the knife-edge is shown in Fig. 19(a). After the distorted image correction, which is described in the Sec. 5, the corrected photo is shown in Fig. 19(b). Extracting the gray value along the white dotted line across the center of the lens in Fig. 19(b),

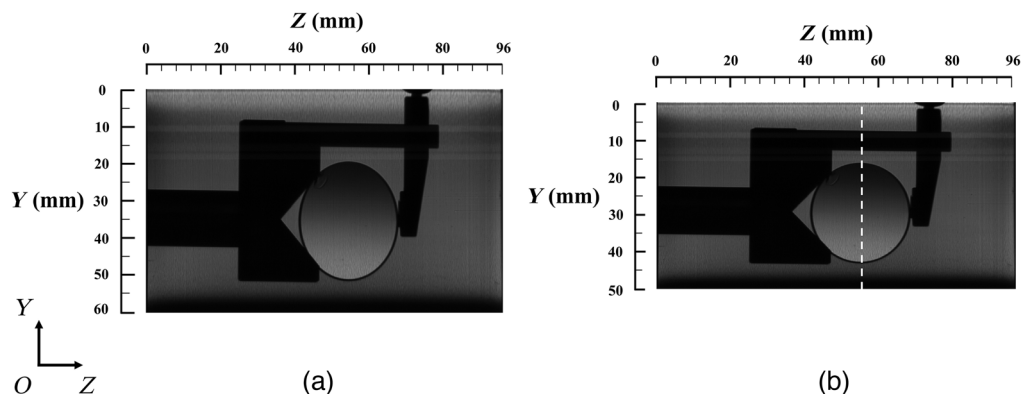


Fig. 19 (a) Original Schlieren photograph and the (b) distortion correction photograph.

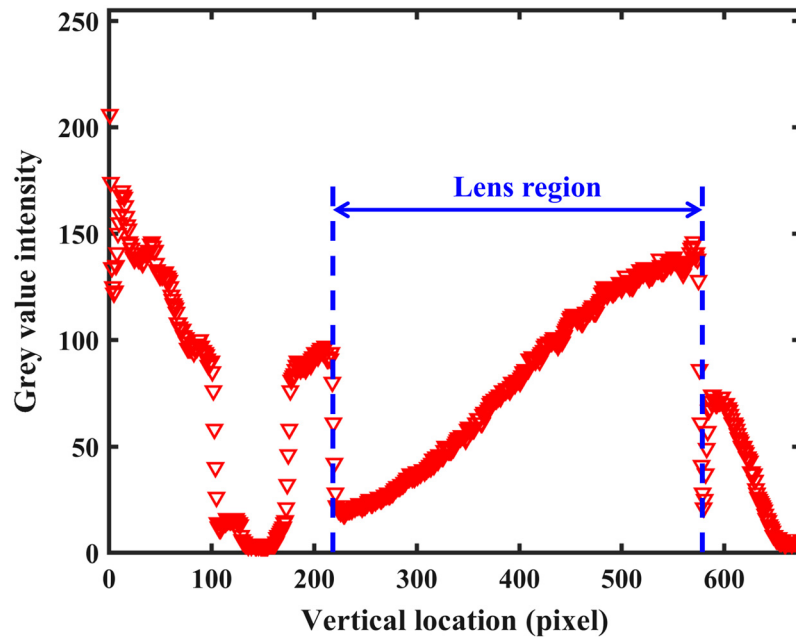


Fig. 20 Gray value intensity with the vertical location.

we show the corresponding gray value intensity on the different vertical locations in Fig. 20. Within the geometric region of the calibration lens, the corresponding ratio value shows a linear relationship. This test results reveals the quasi-quantitative Schlieren measurement effect across the high-precision conformal optical window pair of the cylindrical isolator.

7 Conclusion

In summary, aiming at the quasi-quantitative Schlieren measurement in the cylindrical isolator through the conformal optical window pair, this article adopts both the theoretical, simulation, and experimental methods for the objective research.

First, from the theory of the Schlieren optical measurement, the design requirement of the transmitted wavefront error in the conformal optical windows was presented. Then, from the design of the conformal optical windows, the relationship between the observation region and the window thickness was put forward, providing guidance on maintaining balance between the manufacturing feasibility and the observation performance of the conformal windows. Second, the optical simulation model of the Schlieren measurement and the numerical simulation model of deflection angles through the conformal optical windows of the cylindrical isolator were established for the first time, describing the homogeneity of Schlieren imaging background and the variation of deflection angle ratio with the change of window aberrations for the quasi-quantitative Schlieren measurement. In the next part, based on the actual wind tunnel test conditions, the deformations of conformal optical windows in silica and acrylic materials were first simulated using the fluid-structure interaction method, and the usability of different conformal windows under actual working conditions in the quasi-quantitative measurement field was analyzed. Then, the specific computational model of the distortion correction through the conformal windows was presented, contributing to the image recovery for the quasi-quantitative measurement. Finally, the quasi-quantitative Schlieren measurement with the calibration lens through the conformal optical windows was conducted for the experimental verification.

Acknowledgments

The project was supported by Open Research Fund of State Key Laboratory of High Performance Complex Manufacturing, Central South University (Grant No. Kfkt2020-07).

References

1. E. T. Curran, "Scramjet engines: the first forty years," *J. Propul. Power* **17**(6), 1138–1148 (2001).
2. M. O. Dustin and G. L. Cole, "Performance comparison of three normal-shock position sensors for mixed-compression inlets," NASA TM X-2739 (1973).
3. M. O. Dustin et al., "Continuous-output terminal-shock-position sensor for mixed compression inlets evaluated in wind-tunnel tests of YF-12 aircraft inlet," NASA TM X-3144 (1974).
4. G. F. Orton et al., *Airbreathing Hypersonic Aircraft and Transatmospheric Vehicles*, AIAA (1997).
5. F. S. Billig et al., "Inlet-combustor interface problems in scramjet engines," in *Proc. First Int. Symp. Air Breathing Engines*, International Society for Air Breathing Engines (1972).
6. J. S. Geerts and K. H. Yu, "Visualization of shock train-boundary layer interaction in mach 2.5 isolator flow," in *43rd Fluid Dyn. Co-located Conf.*, June 24-27, San Diego, CA (2013).
7. L. Tian et al., "Study of density field measurement based on NPLS technique in supersonic flow," *Sci. China Ser. G: Phys. Mech. Astron.* **52**, 1357–1363 (2009).
8. G. S. Settles, *Schlieren and Shadowgraph Techniques*, Springer Berlin Heidelberg (2001).
9. G. S. Settles and M. J. Hargather, "A review of recent developments in schlieren and shadowgraph techniques," *Meas. Sci. Technol.* **28**(4), 42001 (2017).
10. T. Fujikawa et al., "Development of transparent cylinder engines for Schlieren observation," *SAE Trans.* **97**(6), 1714–1723 (1988).
11. P. Lin, *Geometric Effects on Precombustion Shock Train in Constant Area Isolators*, AIAA (1993).
12. C. Mauger et al., "Shadowgraph, Schlieren and interferometry in a 2D cavitating channel flow," *Exp. Fluids* **53**(6), 1895–1913 (2012).
13. S. A. Kaiser et al., "Schlieren measurements in the round cylinder of an optically accessible internal combustion engine," *Appl. Opt.* **52**(14), 3433–3444 (2013).
14. T. Ozasa et al., "Schlieren observations of in-cylinder phenomena concerning a direct-injection gasoline engine," SAE Tech. Paper 982696 (1998).
15. B. D. Witt et al., "Optical contouring of an acrylic surface for pipe-flow visualization experiments," in *37th AIAA Plasmadyn. & Lasers Conf.* (2006).
16. D. W. Holder and R. J. North, "Schlieren methods," NPL notes on Applied Science no.31 (1963).
17. R. J. Goldstein, "Optical systems for flow measurement-shadowgraph, schlieren, and interferometric techniques," in Chap. 8 of *Fluid Mechanics Measurements*, pp. 377–422, Springer-Verlag, Berlin (1983).
18. B. D. Witt et al., "Optical contouring of an acrylic surface for non-intrusive diagnostics in pipe-flow investigations," *Exp. Fluids* **45**(1), 95–109 (2008).
19. K. Kozuka et al., "Schlieren observation of spark-ignited premixed charge combustion phenomena using a transparent collimating cylinder engine," *J. Eng. Gas Turbines Power* **125**(1), 336–343 (2003).
20. Y. Ou et al., "Integrative design and processing of a conformal optical window pair in a cylindrical isolator," *Appl. Opt.* **61**(21), 6289–6296 (2022).
21. M. J. Hargather and G. S. Settles, "A comparison of three quantitative schlieren techniques," *Opt. Lasers Eng.* **50**(1), 8–17 (2012).

Biographies of the authors are not available.